# Melt compounding of polypropylene-based clay nanocomposites

Li, J.; Ton-That, M.-T.; Leelapornpisit, W.; Utracki, L. A.



**Publisher's version / Version de l'éditeur:**
https://doi.org/10.1002/pen.20841
*Polymer Engineering and Science, 47, 9, pp. 1447-1458, 2007-08-01*

# Melt Compounding of Polypropylene-Based Clay Nanocomposites

**J. Li, M.-T. Ton-That, W. Leelapornpisit, L.A. Utracki**
*Industrial Materials Institute, National Research Council Canada, 75 Mortagne Blvd, Boucherville, Quebec, Canada J4B 6Y4*

**Polypropylene (PP)-based nanocomposites containing 4 wt% maleic anhydride grafted PP (PP-*g*-MA) and 2 wt% Cloisite 20A (C20A) were prepared using various processing devices, viz., twin-screw extruder (TSE), single-screw extruder (SSE), and SSE with an extensional flow mixer (EFM). Two processing methods were employed: (I) masterbatch (MB) preparation in a TSE (with 10 wt% C20A and clay/compatibilizer ratio of 1:2), followed by dilution in TSE, SSE, or SSE + EFM, to 2 wt% clay loading; (II) single pass, i.e., directly compounding of dry-blended PP-g-MA/clay in TSE, SSE, or SSE + EFM. It has been indicated that the quality of clay dispersion, both at micro- and nanolevel, of the nanocomposites depends very much on the operating conditions during processing, such as mixing intensity and residence time, thus affecting the mechanical performance. Besides that the degradation of the organoclay and the matrix is also very sensitive to these parameters. According to results of X-ray diffraction, field emission gun scanning electron microscopy, transmission electron microscopy, and mechanical tests, the samples prepared with MB had better overall clay dispersion, which resulted in better mechanical properties. The processing equipment used for diluting MB had a marginal influence on clay dispersion and nanocomposite performance.** POLYM. ENG. SCI., 47:1447–1458, 2007. 

## INTRODUCTION

Clay-containing polymeric nanocomposites (CPNC) are composed of polymer matrix and clay with nanoscale dimension [1]. When well dispersed, small amount of clay dramatically improves properties of the CPNC, such as mechanical performance [2, 3], flame retardancy [4–6], chemical resistance [7], dimensional stability [8–10], or gas permeability [11, 12].

The improvement of polymer properties by incorporation of clays is not a new subject [13, 14]. Two findings started renaissance of these materials. The first one was the research on polyamide (PA)-based nanocomposite containing synthetic and natural clays, respectively, at Unitika and Toyota research centers [15–17]. The second one was the series of publications by Vaia based on his graduate work [18] on formation of nanocomposites by static diffusion of molten polymer into clay interlamellar galleries.

The polymer melt intercalation is most valuable industrially, because of its environmentally benign character, versatility, and compatibility with current polymer processing methods. Extensive research efforts have been focused on the performance of nanocomposites prepared by melt compounding. To prepare CPNC with high performance, two steps are important: formulation and processing. The key challenge in compounding nanocomposites is to uniformly disperse clay particles into individual platelets (exfoliation). Since PP macromolecules do not have polar groups, the homogeneous dispersion of hydrophilic clay lamellae in PP is difficult. For this reason, it is necessary to modify clay enhancing its interaction with polymeric matrix. At the same time, the incorporation of compatibilizer into the PP matrix improves miscibility between the organoclay and matrix.

In thermodynamically miscible systems, melt-processing accelerates the dispersion and improves properties of the resulting nanocomposites. Utracki et al. [19] have used twin-screw extruder (TSE) or single-screw extruder (SSE) with an extensional flow mixer (EFM) for preparing polymeric nanocomposites containing Cloisite 15A. The EFM is a device in which extensional flow is intentionally promoted, so that the efficient distributive and dispersive mixing can be achieved. The most important part of device is the convergent–divergent (C-D) plates. The device forces the material to pass a series of C-D elements having three zones: a hyperbolic convergence that orient organoclay aggregates in the flow direction, a controllable gap where the lamellae are peeled off, and a divergent part that randomizes the flow. The most critical is the balance of the extensional to shear stress, engendered within this C-D part.

This paper will present results on the effects of mixing strategies (sample preparation with or without masterbatch step), and compounding devices (TSE, SSE, and SSE +

*Correspondence to*: M.-T. Ton-That; e-mail: minh-tan.ton-that@cnrc-nrc.gc.ca
Contract grant sponsor: Natural Sciences and Engineering Research Council of Canada (NSERC); contract grant number: N00078.
DOI 10.1002/pen.20841
Published online in Wiley InterScience (www.interscience.wiley.com).

TABLE 1. Materials used in these experiments.

| Trade name | $M_w$ (kg/mol) | Density at 25°C (g/ml) | $T_m$ (°C) | MA content (wt%) | Supplier |
|---|---|---|---|---|---|
| PROFAX-PDC1274 (PP) | 250 | 0.902 | ~161 | — | Basell Polyolefins |
| Polybond 3150 (PP-MA) | 330 | 0.91 | ~164 | 0.5 | Crompton Corporation |
| Cloisite® 20A[a] | — | — | — | — | Southern Clay Products |

[a] Cloisite 20A is MMT intercalated with dimethyl dihydrogenated tallow quaternary ammonium chloride (2M2HT) with 39 wt% of organic phase.

EFM) on the degree of dispersion of organoclay in PP matrix and resulting performance.

## EXPERIMENTAL

### *Materials*

Polypropylene (PP, Profax PDC1274) used in this study was from Basell Polyolefins. Maleic anhydride grafted PP, Polybond 3150 (PB3150) from Crompton Corp., was used as a compatibilizer. The nanofiller was organically modified montmorillonite clay, Cloisite® 20A (C20A) form SCP. Table 1 provides more detailed information about these materials.

### *Preparation of Nanocomposites*

**Masterbatch Method.** Prior to extrusion, PB3150 and C20A were dried in a vacuum oven at 90°C overnight. In the first step, PP with 20 wt% compatibilizer (PP-*g*-MA) was dry-blended and fed from hopper, while 10 wt% of organoclay was supplied from a side feeder. The compounding was carried out using a corotating TSE (Leistritz 34 mm CORI, $L/D = 40$; the screw configuration is shown in Fig. 1, top). The side feeder was located at the third segment of the barrel. The processing temperature was set at 200°C from the hopper to the die. The screw speed was 200 rpm and throughput $Q = 5$ kg/h. The compounding was conducted under a blanket of dry $N_2$. The masterbatch (MB) extrudates were palletized for the later use.

In the second step, MB was diluted to 2 wt% of C20A at 190°C, using TSE, SSE, or SSE + EFM. When the dilution was carried out in TSE, the processing parameters were kept the same as for MB preparation. When the dilution was carried out using SSE (Flag 63 mm, $L/D = 24$; with Day mixing screw) or SSE + EFM (gap = 30 $\mu$m), the same processing conditions were used as those for TSE. The lower part of Fig. 1 shows the sequential arrangement of SSE with EFM. Sample prepared in TSE, SSE, or SSE + EFM are designated as TMC20A, SMC20A, and SMC20AE, respectively.

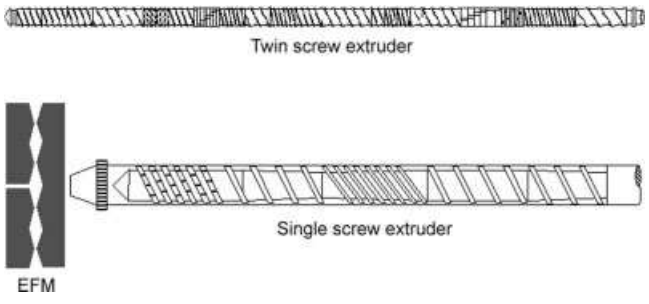


FIG. 1. Illustration of the screws and EFM used for the preparation of nanocomposites. (top) TSE; (bottom) EFM; and SSE.

**Single Pass Method.** Here, the samples were directly compounded in TSE, SSE, or SSE + EFM. Prior to melt compounding, C20A and PP-*g*-MA were dried in a vacuum oven at 90°C overnight. For the better mixing, the PP and PP-*g*-MA mixture was coated with about 0.5 wt% decane and then dry-blended with 2 wt% C20A, by shaking them in a plastic bag for 3 min. The throughput and processing temperature were the same as for the MB method. Samples prepared in TSE, SSE, or SSE + EFM under these conditions are labeled as TNC20A, SNC20A, and SNC20AE, respectively (Table 2).

### *Measurements*

**X-ray Diffraction.** The interlayer spacing, $d_{001}$, was measured in a Brüker D8 Discover with Cu K$\alpha$ radiation. X-ray diffraction (XRD) scans were obtained using an incident X-ray wavelength $\lambda = 0.15406$ nm at a scan rate of 0.6°/min. Two scan ranges were used, one for investigating organoclay spacing ($2\theta = 0.8°$–$10°$) and the other for polymeric matrix crystal structure ($2\theta = 10°$–$30°$). For the $2\theta = 0.8°$–$10°$ the spectra were obtained with slits of 1, 0.1, and 0.6 mm, and for the $2\theta = 10°$–$30°$ with slits of 1 and 1 mm each.

TABLE 2. Identification of samples.

| Sample | Compounding | PB3150 (wt%) | C20A (wt%) |
|---|---|---|---|
| PP | TSE | 0 | 0 |
| PP + PB3150 | TSE | 4 | 0 |
| SNC20A | SSE, direct | 4 | 2 |
| SNC20AE | SSE + EFM, direct | 4 | 2 |
| SMC20A | SSE, MB | 4 | 2 |
| SMC20AE | SSE + EFM, MB | 4 | 2 |
| TNC20A | TSE, direct | 4 | 2 |
| TMC20A | TSE, MB | 4 | 2 |


DOI 10.1002/pen

**Field Emission Gun Scanning Electron Microscopy.** A field emission gun scanning electron microscopy (FEGSEM; Hitachi – 4700) with the working operation voltage of 2 kV was used to observe the microdispersion of the samples. The samples were etched with a mixture of potassium permanganate ($KMnO_4$), phosphoric acid ($HPO_3$), and sulfuric acid ($H_2SO_4$), which removes the amorphous domains and improves the contrast between the clay and the matrix.

**Transmission Electron Microscopy.** The direct observation of organoclay dispersion in CPNC was conducted on a transmission electron microscope (TEM; JEOL JEM 2011) at an acceleration voltage of 200 kV. For TEM measurements ultrathin sections were prepared under liquid nitrogen with a diamond knife using a Leica Ultracut FC microtome. At least three specimens were prepared for each sample, and observation was made at different locations of the specimen.

**Differential Scanning Calorimetry.** A Perkin Elmer Pyris-1 series differential scanning calorimetry (DSC) was employed to examine the crystallization behavior of the specimens. Samples were heated from 30 to 200°C at a rate of 20°C/min and then cooled from 200 to 30°C at the rate of 10°C/min under nitrogen atmosphere. The melt starting temperature ($T_{m,onset}$), and the peak melting temperature ($T_{m,peak}$) were obtained from DSC endotherms; while the crystallization starting temperature ($T_{c,onset}$), peak crystallization temperature ($T_{c,peak}$), and the total crystallinity were obtained from DSC exotherms or endotherms. Crystallinity in specimens used for mechanical testing was calculated from the DSC endotherms from the first heating runs.

**Mechanical Testing.** The tensile test (ASTM D 638) was carried out using the Instron tester (model 1123) at a crosshead speed of 5 mm/min. The flexural tests (ASTM D 790) were performed using Instron tester (model 1124) with the support span of 59 mm and a speed of 15.7 mm/min. The notched Izod impact tests (ASTM D 256) were conducted in a Testing Machine tester, model 8200. All samples were injected having dimensions according to the ASTMs and then conditioned in an oven at 60°C for 24 h prior testing. All of these tests were carried out at room temperature.

## RESULTS

*Dispersion of Organoclay in PP Matrix*

**Dispersion of Organoclay in PP Matrix—Effect of Compounding Method.** The XRD patterns of samples prepared by MB or single pass (S-P) methods are shown in Fig. 2. Based on the XRD data, the $d_{001}$ spacings were calculated from the Bragg's relation—their values are indicated in Fig. 2. For comparison the XRD pattern for pristine C20A is also displayed.

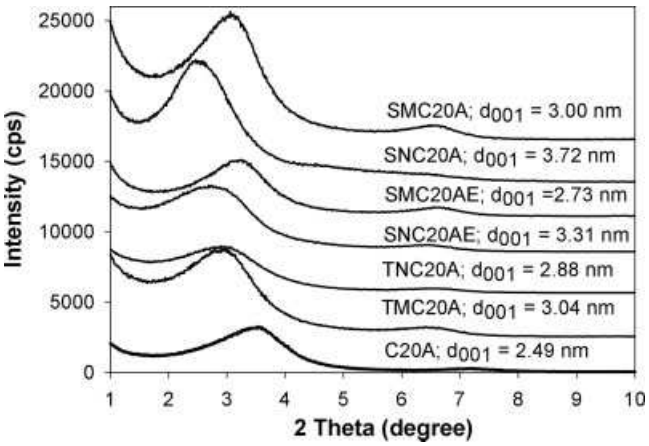


FIG. 2. XRD patterns of pristine organoclay and nanocomposites.

The samples prepared using S-P method in SSE had relatively larger $d_{001}$ spacing (e.g., SNC20A with $d_{001}$ = 3.72 nm) while those from MB method are smaller (e.g., SMC20A with $d_{001}$ = 3.00 nm). The opposite was observed for samples prepared in TSE. With MB method the $d_{001}$ of TMC20A is larger (3.04 nm) than that of TNC20A (2.88 nm).

The FEGSEM micrographs in Figs. 3–5 show the microdispersion in samples prepared using S-P or MB method. Figure 3a and b are images of SNC20A (prepared by S-P method in a SSE), while Fig. 3c and d, are images of SNC20AE (prepared in SSE + EFM). Figure 4a and b are images of SMC20A (prepared by MB method, after dilution in a SSE), and Fig. 4c and d are images of SMC20AE (prepared by MB method, after dilution in SSE + EFM). Figure 5a and b are images of TNC20A (prepared by S-P method in a TSE), and Fig. 5c and d are the images of TMC20A (after diluting MB in a TSE). In general, the nanocomposites prepared by MB method showed better microscale dispersion. In compositions prepared by S-P method a number of large aggregates are present, indicating nonuniform microdispersion.

**Dispersion of Organoclay in PP Matrix—Effect of Compounding Equipment.** The effects of compounding equipment on the degree of dispersion are hidden in Figs. 2–5. The XRD diffractograms in Fig. 2 show coherent scattering of organoclay stacks, and thus offer nanoscale information on the extent of intercalation by macromolecules. Thus, the ones of specimens prepared by MB method in different processing devices show marginal differences of the interlayer spacing, viz. in SMC20A $d_{001}$ = 3.00 nm, in SMC20AE $d_{001}$ = 2.73 nm, and in TMC20A $d_{001}$ = 3.04 nm. Larger variations of $d_{001}$ are observed for the specimens prepared by S-P method in different processing devices, viz. in SNC20A $d_{001}$ = 3.72 nm, in SNC20AE $d_{001}$ = 3.31 nm, and in TNC20A $d_{001}$ = 2.88 nm.

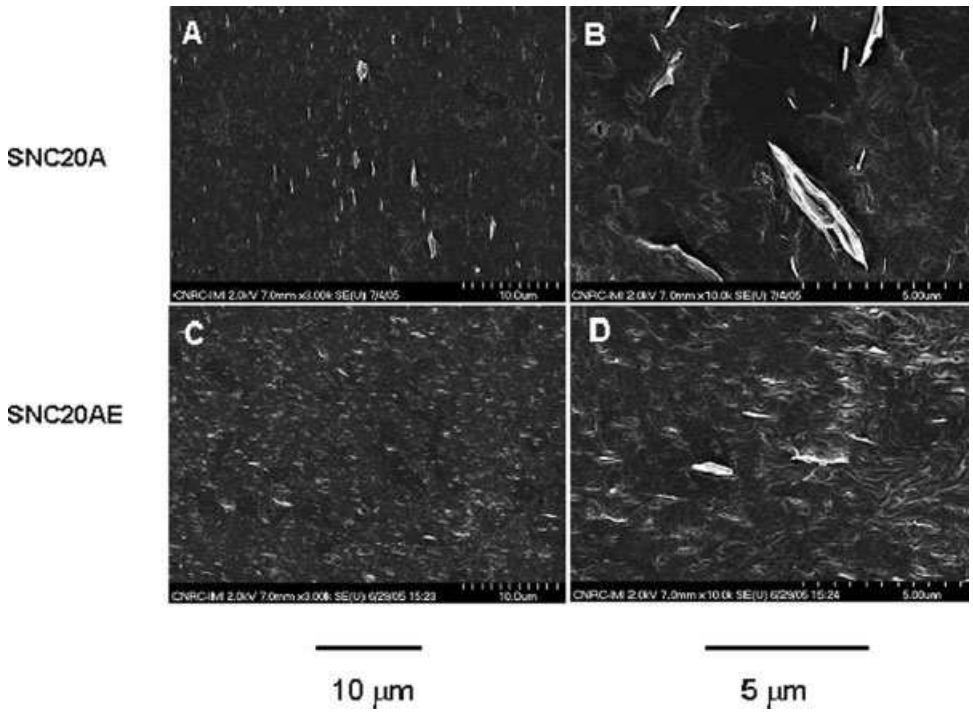


FIG. 3. FEGSEM micrographs for the nanocomposites of SNC20A (a and b) and SNC20AE (c and d).

The effect of compounding equipment on the dispersion of organoclay in PP matrix is also evident in the SEM micrographs of Figs. 3–5. Under the same compounding conditions, better dispersion was observed in samples compounded in TSE or SSE + EFM, than in SSE alone.

The intercalated/exfoliated structures and the degree of C20A dispersion can also be assessed from the TEM images. In Fig. 6, micrographs of TMC20A and SMC20AE at three magnifications are shown. Both these samples were prepared by MB method, the former in a TSE, the latter in SSE + EFM. The dark features origi-

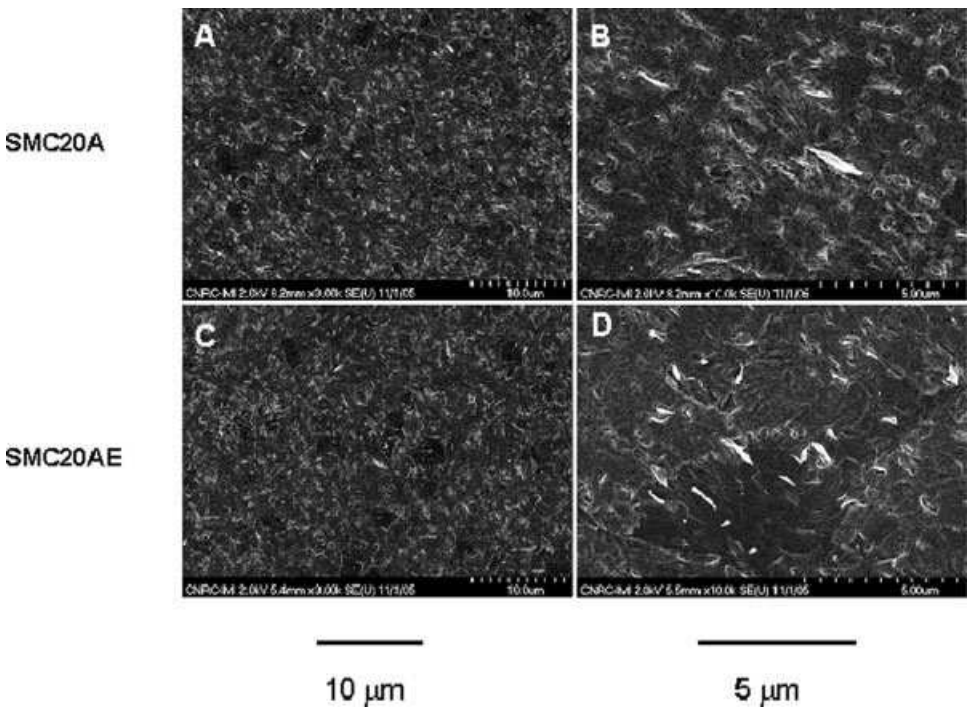


FIG. 4. FEGSEM micrographs for the nanocomposites of SMC20A (a and b) and SMC20A (c and d).

 DOI 10.1002/pen

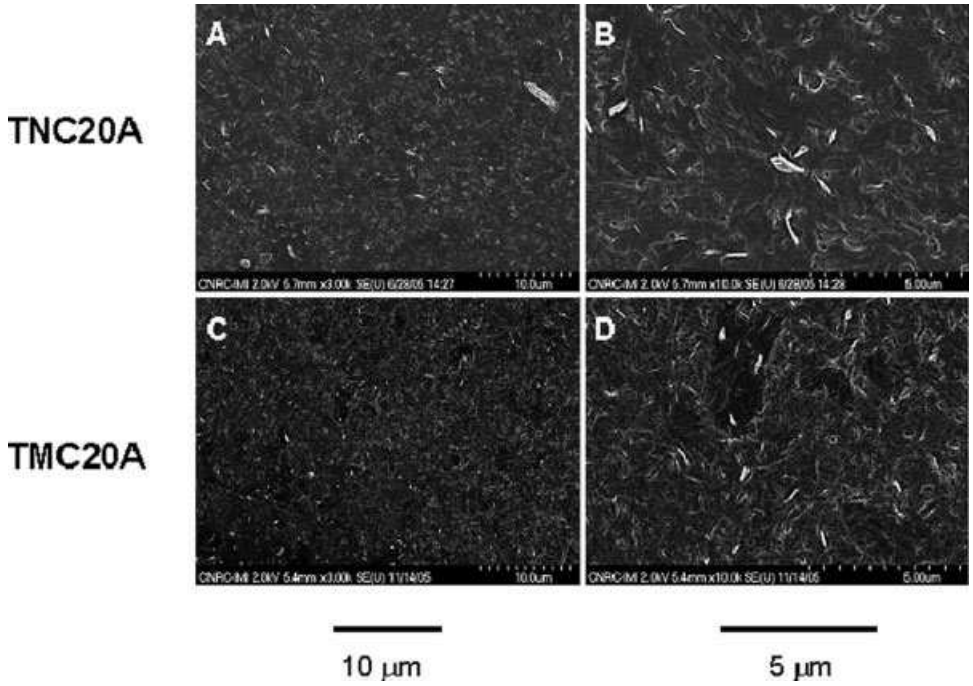


FIG. 5. FEGSEM micrographs for the nanocomposites for TNC20A (a and b) andTMC20A (c and d).

nate from clay stacks or perpendicularly aligned double or single platelets. The two low-magnification images demonstrate that dilution in TSE resulted in numerous small stacks containing several platelets. The stacks in the sample diluted in SSE + EFM are of similar size, but less numerous and less tightly packed. Unlike the random stacks dispersion in TMC20A, these in SMC20AE are oriented. On zooming to the highest magnification, both "short" stacks and individual platelets might be observed. For reasonably comparing XRD results with the TEM observations, the micrographs at several locations were obtained. In average, the distance between the two clay layers in these micrographs is in TMC20A ~3.0 nm (Fig. 6c) and in SMC20AE ~2.7 nm; these results are consistent with the XRD data.

*Crystallinity*

The effect of addition of organoclay on the crystallization behavior of the matrix was studied using DSC and XRD method. Figure 7 shows the DSC heating and cooling curves. Table 3 summarizes the results, listing the onset melting temperature $T_{m,onset}$, peak melting temperature, $T_{m,peak}$, initial crystallinity (first heating) and crystallinity after cooling.

It has been well documented that isotactic PP can exhibit $\alpha$, $\beta$, and $\gamma$ crystal forms depending on the crystallization conditions and the addition of nucleating agents. Figure 8 displays XRD patterns of the specimens in the range $2\theta = 10°–30°$. All specimens show $\alpha$ (110) and $\alpha$ (030) peaks in this range. The location of the respective peaks is indistinguishable among the samples. Excepting SMC20A and SMC20AE, all other specimens also show $\beta$ peak.

*Mechanical Properties of PNC*

The effect of MB and S-P compounding methods and that of the compounding devices on the tensile properties of CPNC is presented in Fig. 9. All the samples (prepared by MB or S-P method) have higher tensile modulus than PP or PP + PP-*g*-MA, indicating the reinforcing effect of the clay. The flexural properties (not shown) follow similar dependence. Furthermore, the tensile and flexural properties of samples prepared by MB method are superior to those prepared by the S-P one. The impact strength of PP and PNCs is shown in Fig. 10. All values are higher than that of PP or PP + PP-*g*-MA.

## DISCUSSION

*Clay Dispersion in PP Matrix*

As evident from data in Fig. 2, compounding increases the interlayer spacing, but the increase depends on the processing method and device. For the MB method and dilution in TSE the $d_{001}$ value of TMC20A increased from that of C20A (2.49–3.04 nm). Similarly, for the MB method and dilution in SSE or SSE + EFM, $d_{001} = 3.00$ and 2.73 nm for SMC20A and SMC20AE, respectively. For the S-P method, the $d_{001}$ value for TNC20A is 2.88 nm, while that for the SNC20A and SNC20AE is $d_{001} = 3.72$ and 3.31 nm, respectively.

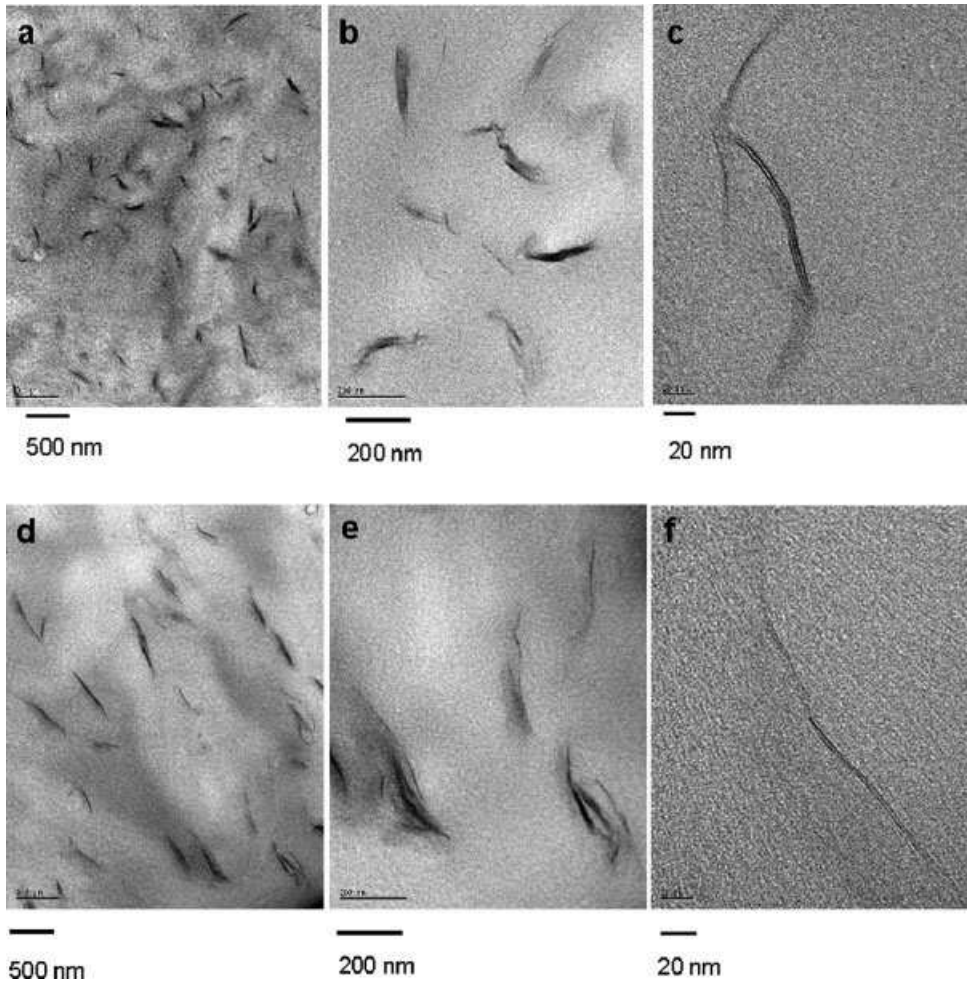


FIG. 6. TEM micrographs for the PNCs of TMC20A and SMC20AE. (a) TMC20A at low magnification, (b) TMC20A at medium magnification, (c) TMC20A at high magnification, (d) SMC20AE at low magnification, (e) SMC20AE at medium magnification, and (f) SMC20AE at high magnification.

At the first glance, these results are contrary to expectation because high concentration of compatibilizer and organoclay during MB preparation should enhance the interaction between the compatibilizer and organoclay, and thus lead to better intercalation than when using S-P method. However, it is apparent that the organoclay intercalation is closely related with the processing device. In the case of compounding in SSE, the processing conditions are milder than those in TSE. The mild conditions and longer residence time in SSE (than in TSE) enables the compatibilizer to diffuse into the interlayer galleries. When EFM is added to SSE, the $d_{001}$ of SNC20AE

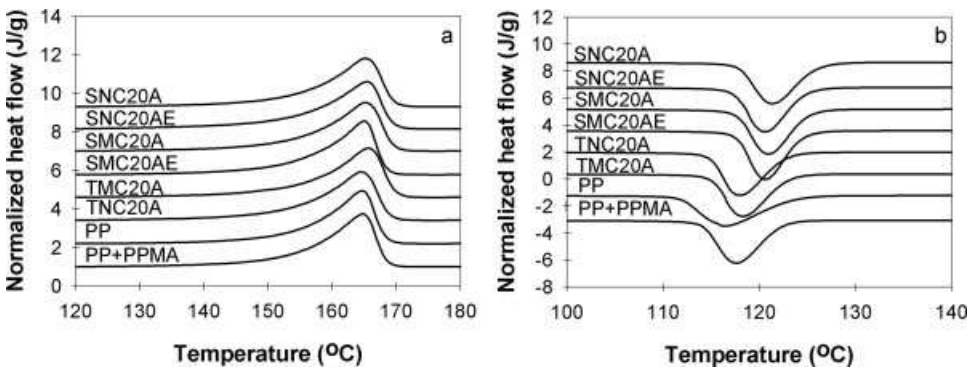


FIG. 7. DSC thermograms of PP, PP-*g*-MA, and nanocomposites. (a) Heating scans at the rate of 20°C/min and (b) cooling scans at the rate of 10°C/min.

 DOI 10.1002/pen

TABLE 3. DSC data for the specimens.

| Sample | $T_{m,onset}$ (°C) | $T_{c,onset}$ (°C) | $T_{m,peak}$ (°C) | $T_{c,peak}$ (°C) | Crystallinity, heating (%) | Crystallinity, cooling (%) |
|---|---|---|---|---|---|---|
| PP | 155.0 (±0.2) | 117.2 (±0) | 165.2 (±0.2) | 111.9 | 40.1 (±0.4) | 45.6 (±1.1) |
| PP + PB3150 | 155.4 (±1.8) | 117.4 (±0.2) | 165.3 (±0.4) | 112.3 (±0.7) | 40.9 (±0.6) | 45.6 (±1.2) |
| SNC20A | 156.0 (±1.2) | 126.1 (±0.2) | 165.4 (±0.7) | 121.6 (±0.7) | 40.0 (±0) | 45.8 (±0.1) |
| SNC20AE | 154.4 (±0.3) | 124.9 (±0) | 165.4 (±0.7) | 120.7 (±0.4) | 40.7 (±0.1) | 45.3 (±0.2) |
| SMC20A | 154.5 (±0.7) | 125.2 (±0.2) | 165.2 (±0.1) | 121.8 (±1.2) | 40.7 (±0) | 44.9 (±0.6) |
| SMC20AE | 155.6 (±0.1) | 124.1 (±0.6) | 165.2 (±0) | 119.9 (±1.0) | 40.9 (±0.1) | 45.8 (±0.8) |
| TNC20A | 156.0 (±1.2) | 123.2 (±0.2) | 165.4 (±0.7) | 118.5 (±0.5) | 40.0 (±0) | 46.4 (±1.8) |

slightly decreased. This effect might originate in high pressure gradient in EFM and resulting extensional and shear stresses. The lowest $d_{001}$ spacing was observed for the sample TNC20A. Obviously, short residence time can be responsible for the incomplete intercalation. For the samples prepared by MB method, the interlayer spacings were similar.

The data in Fig. 2 strongly suggest that the intercalation by PP-*g*-MA compatibilizer is relatively rapid and efficient, increasing the intergallery distance by ≥1.23 nm—sufficient for the formation of a double layer. However, simultaneously, with the intercalating diffusion of PP-*g*-MA, the Hofmann elimination process [20] takes place, causing the quaternary ammonium ions to decompose, which reduces the spacing—the greatest damage is done by high shearing in a TSE (at $T = 190$ and 200°C the effect is similar), the mildest is in a SSE, with the SSE + EFM effects in between.

It is noteworthy that MB was compounded in a TSE with relatively short residence time of 94 s, which limited the diffusion effects. Thus the main mechanism of clay dispersion in the molten polymeric matrix was shearing and peeling clay platelets from stacks. Comparing the $d_{001}$ values of SMC20A, SMC20AE, and TMC20A, the results indicate that during dilution Hofmann elimination compensated for the additional intercalation. According to the XRD patterns, the order of intercalation level follows the sequence: SNC20A > SNC20AE > TNC20A for the S-P method, and TMC20A > SMC20A > SMC20AE for the MB method.

Independently whether during the dilution stage $d_{001}$ spacing increases or not, the potential peeling mechanism might still increase the number of individual clay platelets within the matrix, improving the degree of exfoliation. This mechanism may be more important for improving the CPNC performance than the spacing in short stacks itself. In Fig. 2 the exfoliation effect is evidenced by the relative magnitude of the main peak. The area under the peak is related to that fraction of organoclay that remains in the form of stacks, i.e., the larger the peak the smaller the percentage of exfoliated clay. The degree of dispersion obtained using SSE alone (MB or S-P method) was lower than when using TSE (MB method), SSE + EFM (MB or S-P method).

While XRD reflects on the degree of clay dispersion on the nanoscale, the FEGSEM in Figs. 3–5 provides supplementary information on microdispersion, i.e., on the presence or absence of organoclay aggregates. The images presented in Figs. 3–5 clearly indicate that the dispersion of the samples prepared by MB method is superior to that prepared by S-P one. The function of EFM is to enhance the peeling of clay platelets from the stacks thus improving the clay dispersion and distribution. From the earlier images, one should note that the dispersion improvement

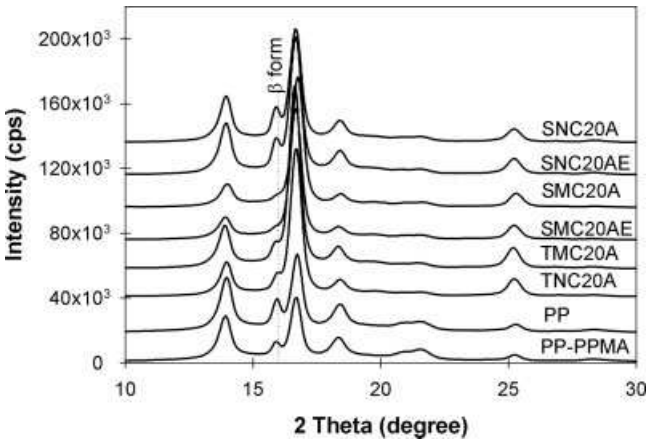


FIG. 8. XRD patterns of PP, PP-*g*-MA, and nanocomposites for crystal structure verification.

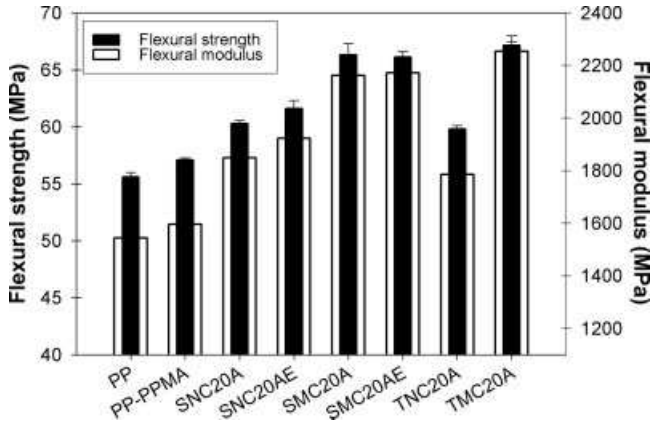


FIG. 9. Tensile modulus and tensile strength at room temperature of PP, PP-*g*-MA, and nanocomposites.

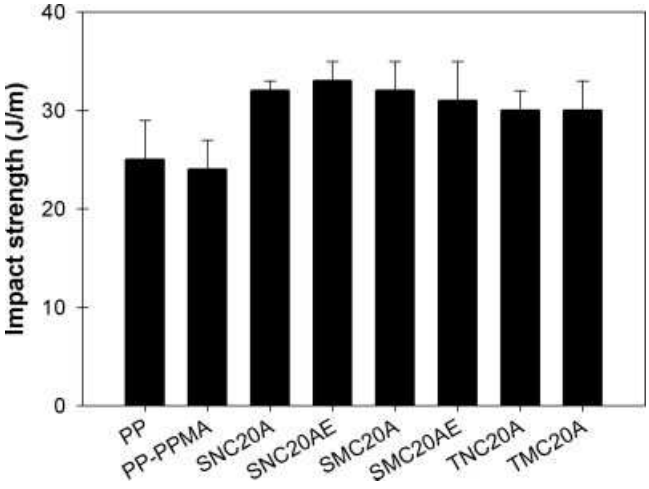


FIG. 10. Notched Izod impact strength at room temperature of PP, PP-*g*-MA, and nanocomposites.

level by EFM depends on the processing method. Comparing micrographs a and b with c and d in Figs. 3 and 4 makes it evident that EFM has a beneficial role for elimination of aggregates. Comparison of Fig. 3 with Fig. 4 indicates that the MB gives better dispersion than the S-P method. The micrographs in Fig. 5 make it evident that the two-stage TSE compounding (MB method) resulted in better dispersion than the single-stage one (S-P method). In short, comparing the micrographs in Fig. 5 with those in Figs. 3 and 4 leads to the conclusion that the worst degree of aggregate elimination was achieved using S-P method in SSE, that EFM attachment to SSE resulted in their elimination comparable to that obtained using TSE (S-P method). The most uniform dispersion was obtained using TSE and the MB method.

Combining the information obtained from XRD and FEGSEM, two effects are to be noted for the samples prepared using SSE + EFM. Under the used compounding conditions, on the one hand, large aggregates were significantly reduced and the resulting organoclay particles appeared to be uniformly distributed. On the other hand, as previously noted, flow through EFM caused some reduction of $d_{001}$ spacing indicating intercalant degradation. Nevertheless, the EFM demonstrated significant improvement of the clay dispersion on the microscale during the melt compounding, especially in the S-P method.

TEM micrographs in Fig. 6 illustrate the extent of C20A intercalation and exfoliation in PP matrix, in samples prepared by MB method with dilution either in TSE or SSE + EFM. The TEM image of TMC20A at low magnification (Fig. 6a) shows that organoclay particles are well dispersed. At higher magnification (Fig. 6b), both intercalated stacks and a few individual layers are evident. The distance between the two layers in an intercalated stack is around 3 nm (Fig. 6c). This result is consistent with the XRD observation for TMC20A. The nanodispersion of SMC20AE is illustrated in Fig. 6d–f. Similar to TMC20A, Fig. 6d also shows a mixed morphology of SMC20AE with intercalated and exfoliated structures.

The information on the degree of dispersion on the nano- and microscale is summarized in Table 4. In the Table the extent of exfoliation and aggregation are listed using a qualitative scale of 1–10; thus for exfoliation, 1 means highest exfoliation and 10 means poorest, while for aggregates, 10 means most aggregates and 1 their absence. Similarly, in the Table 4 the relative extrusion intensity ($N$) is listed—these numbers were calculated assuming that the relative intensity in SSE is the lowest ($N = 1$) and that in TSE = SSE + EFM ($N = 2$).

The three measures of dispersion ($d_{001}$, Exfoliation, and Aggregates) in Table 4 show no clear correlation between the relative exfoliation and $d_{001}$. However, as shown in Fig. 11, they do correlate with extrusion intensity, represented by the parameter $N$. As it could be expected, the number of aggregates decreases with $N$. The opposite is seen for the interlayer spacings—the larger $N$ the smaller $d_{001}$. The estimated degree of exfoliation shows a more complex behavior, initially increasing with $N$, and then at high intensity decrease. Evidently, the intergallery spacing in short stacks is dominated by degradative behavior of the quaternary ammonium ion intercalant of the organoclay (Hofmann elimination mechanism), and as $d_{001}$ decreases the peeling mechanism becomes more difficult.

Recently, Lertwimolnun and Vergnes [21] used TSE for compounding CPNC similar to the one discussed in this paper. From the numerical simulation of the extrusion process the authors deduced that the degree of clay dispersion mainly depends on strain. This conclusion is in accord with results of earlier studies of CPNC dispersion of Cloisite® 15A in PA-6 matrix using several extruders at constant throughput [22]. However, when compounding takes place in shear and elongation, this conclusion may

TABLE 4. Summary of clay dispersion data and relative tensile modulus.

| Sample | XRD, $d_{001}$ (nm) | Exfoliation, Nx | Aggregates, Ag | Intensity, $N$ | Relative modulus, $E_R$ | Relative modulus error | $E_R$ (4) calc | $E_R$ (4) error |
|---|---|---|---|---|---|---|---|---|
| SNC20A | 3.72 | 6.45 | 10 | 1 | 1.22 | 0.05 | 1.180 | 0.0007 |
| SNC20AE | 3.31 | 5.14 | 5 | 2 | 1.24 | 0.05 | 1.206 | 0.0074 |
| SMC20A | 3.0 | 5.27 | 5 | 3 | 1.39 | 0.05 | 1.346 | 0.0046 |
| SMC20AE | 2.73 | 5.50 | 3 | 4 | 1.31 | 0.06 | 1.310 | 0.0076 |
| TNC20A | 2.88 | 5.32 | 6 | 2 | 1.25 | 0.02 | 1.189 | 0.0120 |
| TMC20A | 3.04 | 5.02 | 2 | 4 | 1.36 | 0.04 | 1.373 | 0.0089 |

 DOI 10.1002/pen

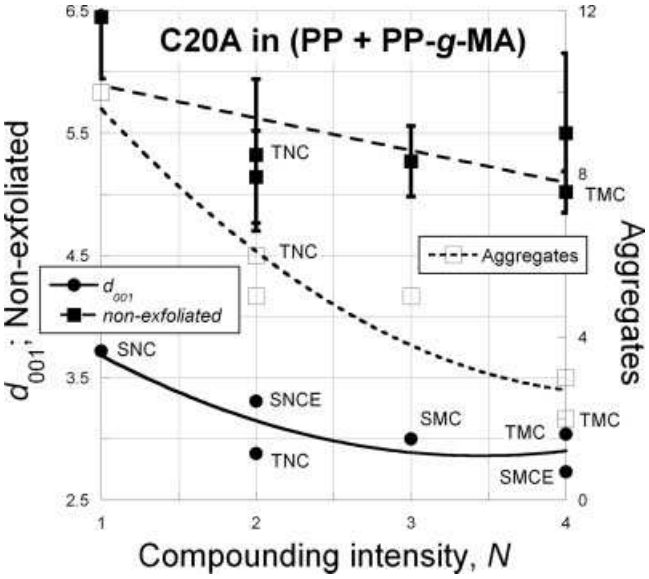


FIG. 11. Three measures of the clay degree of dispersion: $d_{001}$, the relative number of aggregates, and the relative amount of exfoliation are plotted vs. extrusion intensity—see text. The numbers near the data points are for sample identification (listed in Table 4).

not be correct. It suffices to note that the elongational strain depends only on the convergence ratio [23], while the experiments demonstrate that the degree of dispersion to a great extent is affected by the geometry of the convergence [19]. Thus, in this paper an arbitrary extrusion intensity parameter $N$ was used instead of strain.

Finally, it is noteworthy that in agreement with earlier observations [24, 25] better clay dispersion was obtained for samples prepared following the MB method than that of S-P. For similar systems as the one discussed in this paper, the earlier publications reported that the double-extrusion (MB) method resulted in better dispersion than S-P one. However, the advantages vanished if during the dilution stage high-shear TSE screws were operated at too high speed (e.g., 300 rpm), which resulted in thermal degradation and a partial collapse of the interlayer spacing.

### *Crystallinity*

Results of DSC heating and cooling scans are summarized in Table 3, while the XRD information on the crystalline cell structure is presented in Fig. 8. It is evident that addition of organoclay did not change significantly the total crystallinity ($X$ = 40.0–40.9%) or the melting peak position ($T_{m,peak}$ = 165.2–165.8°C), but did increase the crystallization peak temperature from about 112°C to (120.5 ± 0.5)°C. The addition of the clay accelerates crystallization by the heterogeneous nucleation. At an early stage of crystallization, molten PP might be in contact with the clay surface, which leads to the crystallization of PP molecule at a higher temperature. This phenomenon is similar to that described earlier [26]. However, the small variations of $T_{c,peak}$ does not correlate with any measure of clay dispersion in Table 4.

There are small changes in the intensity of $\beta$ peak, which are quite evident in PP, SNC20A, and SNC20AE, apparent as a shoulder in TNC20A and TMC20A, and absent in SMC20A and SMC20AE. One would expect that the presence of the $\beta$ crystalline form might depend on the degree of clay dispersion, but again there is no correlation with any measure of dispersion in Table 4. However, there seems to be some logic in this behavior—the most intensive is the peak for neat PP, and in samples prepared in SSE following the S-P method; hence the mild compounding seems to preserve the $\beta$ form. Presence of a shoulder in TSE S-P compounding could mean that here the compounding conditions are more severe than in SSE, which is reasonable. Now, considering the MB method, the absence of this peak after compounding in SSE seems to follow the logical sequence, but shoulder peak after TSE compounding does not.

### *Mechanical Properties*

**Effect of Matrix Crystallinity on Mechanical Performance.** It might be expected that mechanical properties are affected by the extent of crystallinity. As shown in Fig. 7 and Table 3, the crystallization temperatures of PNCs are higher than that of neat matrix. Incorporation of organoclay (1.2 wt% of MMT) increased the onset of the crystallization, $T_{c,onset}$, by 6–9°C, i.e., clay accelerates crystallization by the heterogeneous nucleation effects. At an early stage of crystallization, the molten PP might be in contact with the clay surface, which leads to the crystallization of PP molecule at a higher temperature. However, the $T_{m,onset}$, $T_{m,peak}$, and crystallinity from either heating or cooling cycle are all similar, apparently unaffected by the clay addition. A possible explanation might be that although at the early stage of crystallization the clay acts as a nucleating agent, thus increasing the rate of crystallization, the type and amount of the crystallizable polymer remains unchanged (as the XRD data shown). Owing to enhanced nucleation, the size of the crystals becomes smaller in the presence of organoclay. This phenomenon is similar to that described earlier by Li et al. [26]. Thus, since the CPNC crystallinity (first heating data) is nearly constant, (40.5 ± 0.5)%, its effect on mechanical performance might be neglected.

**Effect of Clay Dispersion on Tensile Modulus.** The effect of clay dispersion on mechanical performance can be compared with the predictions which have been proposed in [1] as

$$E_R = E_c/E_m = 1 + 0.2w \quad (1)$$

where $E_R$ is the relative modulus; $E_c$ the modulus of CPNC; $E_m$ the modulus of polymer matrix; and $w$ is the clay concentration. Thus for the PNC-containing 2 wt%

C20A (1.36 wt% mineral), the Young's modulus is expected to increase by about 27%. Since the $E_m$ of PP with 4 wt% PP-*g*-MA is 1.73 ± 0.1 GPa, the value of its PNC should be about 2.2 ± 0.1 GPa. For S-P method using SSE alone, the value of SNC20A was determined as 2.11 ± 0.07 GPa, and SNC20AE, 2.15 ± 0.07 GPa. For the same S-P method using TSE, the TNC20A has a value of $E_c$ = 2.16 ± 0.21 GPa. A better enhancement was observed for the samples prepared by MB method using SSE alone, SSE + EFM, or TSE. The obtained values range from 2.40 ± 0.08 GPa for SMC20A to 2.27 ± 0.09 GPa for SMC20AE, and 2.36 ± 0.05 GPa for TMC20A. As shown in Table 4, the average value of relative modulus is $E_R$ 1.31 ± 0.04, in close agreement with the expected value from *Eq. 1*: $E_R = 1.27$.

It is tempting to determine which one of the dispersion parameters significantly affects $E_R$. The task is difficult since the experimental values for constant composition change but little, viz. $E_R$ = 1.22–1.39. To determine the principal variable(s) a linear regression was carried out for the relation:

$$E_R = 1 + a_0 d_{001} + a_1 \mathrm{Nx} + a_2 \mathrm{Ag} + a_3 N \qquad (2)$$

Results of the linear regression for the independent variables are displayed in Fig. 12. Since there are only six data points, for a meaningful correlation, the number of independent variables should be as small as possible. It is noteworthy that for 2–4 variables the determination coefficient DC > 0.8, indicating good correlation of variables. Evidently, when the number of independent variables increases so does DC, $r^2$, etc.—the description of data becomes more precise. Results of these computations are compared with the experimental values of $E_R$ in Fig. 12. In this Figure (as in Fig. 11) the numbers refer to Sample number in Table 4.

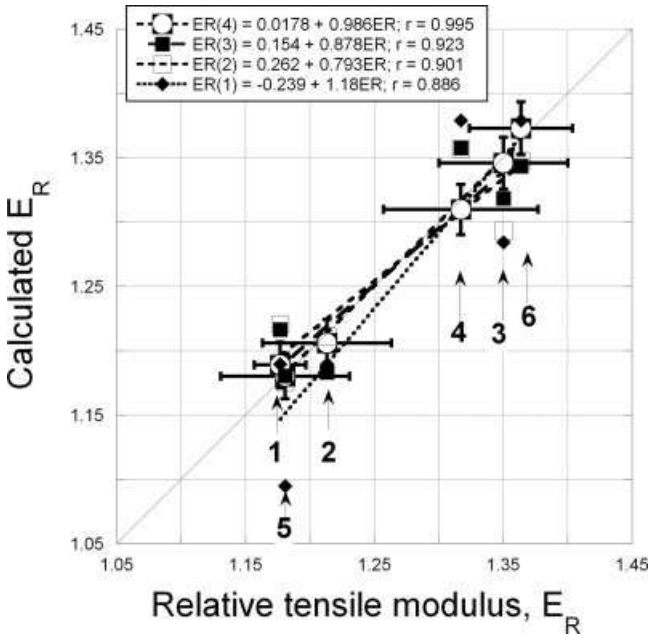


FIG. 12. Calculated from *Eq. 2* relative modulus vs. its experimental value. The number of independent variables varied from one, ER (1), to four, ER (4). The error bars are indicated only for the ER (4) regression. The numbers 1–6 are for sample identification (listed in Table 4).

Evidently *Eq. 2* with four independent variables leads to excellent description of tensile modulus. The description worsens as the number of independent variables decreases. The regression analyses for <4 variables was carried out for all possible combinations—the listed parameters represent the best fit for given group for 3, 2, or 1 parameter. The analysis indicates that $E_R$ mainly depends on the compounding intensity and the number of aggregates, which in turn also depend on *N*. However, one must ask whether the good agreement represents only a curve fitting to linear equation, or it represent the true physics.

First of all, the importance of the processing parameter *N* should be stressed—it correlates independently with $d_{001}$, the number of aggregates, and the relative number of platelets in stacks, but in addition, it also enhances the tensile modulus (viz. all values of $a_3 > 0$) by another mechanism than the mentioned three. Since the processing refers to compounding and not to injection–molding, this additional and important influence is not related to orientation. Since the effect is positive it is not related to the thermochemical degradation, and not, as discussed earlier, to crystallinity. The data in Fig. 11 show that $d_{001}$ decreases with the process intensity, and the most probable reason for it is a progressive degradation of intercalant. Furthermore, enhanced compounding intensity leads to better homogenization of the PP + PP-*g*-MA matrix. It is reasonable to speculate that partial elimination of immiscible intercalant from the clay surface would benefit the polar PP-*g*-MA to diffuse into the gallery of organoclay and result in better matrix–clay interaction. These interactions are expected to reduce the free volume and cause formation of immobilized PP layer on the clay surface [27].

Judging by the positive values of $a_0$ increase of the interlayer spacing improves modulus, while the negative values of $a_1$ logically indicate that improved exfoliation also has a positive effect on CPNC stiffness. The $a_2 > 0$ is unexpected—it simply says that aggregates have a small positive effect on modulus. This certainly seems to be an artifact of the regression method.

**Effect of Clay Dispersion on Tensile Strength.** The tensile strength of SNC20A and SNC20AE is slightly lower than those of PP and PP + PP-*g*-MA, which most likely is due to the presence of large clay aggregates seen in Fig. 3. After adding the EFM to the SSE, the dispersion is improved but it remained poor—a common feature of the samples prepared by S-P method. The large clay aggregates are responsible for engendering weak interphase with the polymer matrix, which under stress initiates fracture and results in low tensile strength. The ten-

 DOI 10.1002/pen

sile strength of TNC20A prepared using TSE is higher than that of SNC20A and SNC20AE. The SEM photo of TNC20A presented in Fig. 4 shows a better microdispersion compared to those of SNC20A and SNC20AE (Fig. 3), indicating the absence of large aggregates. Higher tensile strength was observed for the samples prepared by the MB method. In general, the mechanical properties (tensile and flexural moduli) of the PNC samples increase by about 10% compared to those of PP and PP-PP-*g*-MA. Evidently, better dispersion resulted in better mechanical properties. However, it should be noted that the tensile properties of the samples via MB method are less related to the processing devices used for the dilution step. These observations can be easily analyzed using a similar method to that applied to the tensile modulus.

The influence of the degree of dispersion and method of processing on the relative strength, $\sigma_R$, was examined by the regression analysis. As before, four "independent" variables were used: the interlayer spacing, $d_{001}$, the degree of nonexfoliation, Nx, the relative number of aggregates, Ag, and the intensity of processing, $N$:

$$\sigma_R = 1 + b_0 d_{001} + b_1 \mathrm{Nx} + b_2 \mathrm{Ag} + b_3 N \qquad (3)$$

The correlation of $\sigma_R$ with all 4, with 3, with 2, and with 1 variable was examined. The computational results illustrated in Fig. 13 represent the best correlation within each of these categories, e.g., by contrast with modulus, for two variables better correlation was found with Nx and $N$, than with Ag and $N$. Similarly, for a single variable, the relative processing intensity, $N$, gave the best correlation.

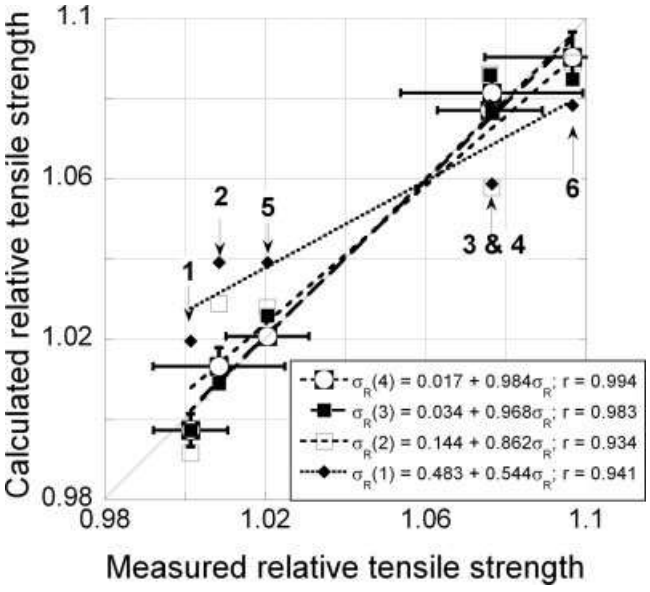


FIG. 13. Calculated from *Eq. 3* relative tensile strength vs. its experimental values. The number of independent variables varied from one, $\sigma_R$ (1), to four, $\sigma_R$ (4); The error bars are indicated only for the $\sigma_R$ (4) regression. The numbers 1–6 are for sample identification (listed in Table 4).

The results of the regression analysis resulted in expected values of the parameters, $b_i$. Strength is mainly controlled by the compounding intensity, supporting the previously proposed mechanism. The influence of $d_{001}$ and Ag is smaller than that of the degree of exfoliation.

**The Impact Strength.** The notched Izod impact strength of the PNCs was found superior to that of PP or PP + PP-*g*-MA, thus while its value for the matrix (PP + PP-*g*-MA) was NIRT = 24 ± 3 J/m, that for CPNCs ranged from 30 to 33 with an average error of measurements ±2 J/m. The improvement caused by incorporation of organoclay is evident in Fig. 9b. The regression analysis indicates a weak correlation only with $d_{001}$.

Yuan and Misra [28] studied the impact fracture of PP-based CPNCs with Nanomer 1.44P. The authors reported a similar behavior. There are two mechanisms affecting the impact fracture: initiation and propagation. In neat PP the fracture initiation and propagation is characterized by crazing and vein-type features. By contrast, for PP-based CPNCs the fracture follows the microvoid–coalescence–fibrillation process. On the basis of the present results, it seems that the microvoid–coalescence is not sensitive to the microdispersion of organoclay in PP matrix. For all of the samples, the enhancement level for the impact strength is quite similar.

## CONCLUSIONS

From the obtained results, several conclusions can be made as follows. Addition of C20A to PP + PP-*g*-MA matrix accelerated its crystallization, but did not affect significantly the crystallinity content and the crystalline structure. Therefore, the variation in mechanical properties of the nanocomposites prepared from the same ingredients was mainly due to the degree of clay dispersion and the degradation of the matrix during mixing (shear intensity and temperature).

The degree of clay dispersion may be described in terms of four parameters: $d_{001}$, extent of exfoliation, number of clay platelets in stacks—all calculated from the XRD data, and the number of aggregates calculated from FEGSEM (microdispersion). These parameters were found to be related to the mixing intensity and the residence time. Longer residence time insured better intercalation and exfoliation, while greater intensive mixing in TSE and in SSE + EFM tended to increase the microdispersion, exfoliation, and matrix degradation but reduce $d_{001}$ due to organoclay degradation (Hofmann mechanism).

In general, the mechanical performance was also related to the degree of dispersion and the mixing intensity power $N$. The linear regression analysis indicated that the relative tensile modulus is dominated by $N$ and the number of aggregates (microdispersion), while the relative tensile strength is more dependent on $N$ and the degree of exfoliation. Furthermore, the samples prepared with MB method exhibited better mechanical properties than those

with S-P method in terms of tensile performance, viz. 35.7 ± 0.2 MPa vs. 32.6 ± 0.1 MPa for tensile strength and 2399.8 ± 79.6 vs. 2113.0 ± 65.9 MPa for tensile modulus. There is no significant difference in impact strength between MB and S-P methods, viz. 31.50 ± 2.0 J/m. Nevertheless, the impact strength of all the CPNC samples was significantly higher than that of the matrix, viz. 31.5 ± 2.0 J/m vs. 24 ± 3 J/m.

## ACKNOWLEDGMENTS

Post doctorate fellowship for J. Li is gratefully acknowledged.

## REFERENCES

1. L.A. Utracki, *Clay-Containing Polymeric Nanocomposites*, Rapra Technology, Shawbury, UK (2004).
2. C. Zilg, P. Reichert, F. Dietsche, T. Engelhardt, and R. Mülhaupt, *Kunstst. Plast. Eur.*, **10**, 1812 (1999).
3. P.C. Lebaron, Z. Wang, and T.J. Pinnavaia, *Appl. Clay Sci.*, **15**, 11 (1999).
4. R.A. Vaia, G. Price, P.N. Ruth, and H.T. Lichtenhan, *J. Appl. Clay Sci.*, **15**, 67 (1999).
5. M. Zanetti, T. Kashiwagi, L. Falqui, and G. Camino, *Chem. Mater.*, **14**, 881 (2002).
6. J. Zhu and C.A. Wilkie, *Polym. Int.*, **49**, 1158 (2000).
7. C. Chen and D. Curliss, *Nanotechnology*, **14**, 643 (2003).
8. J.W. Gilman, *Appl. Clay Sci.*, **15**, 31 (1999).
9. T. Lan, P.D. Kaviratna, and T.J. Pinnavaia, *Chem. Mater.*, **6**, 573 (1994).
10. Y. Yang, Z. Zhu, J. Yin, X. Wang, and Z. Qi, *Polymer*, **40**, 4407 (1999).
11. R. Xu, E. Manias, A. Snyder, and J. Runt, *Macromolecules*, **34**, 337 (2001).
12. P.B. Messersmith and E.P. Giannelis, *J. Polym. Sci. Part A: Polym. Chem.*, **33**, 1047 (1995).
13. B. Theng, *Formation and Properties of Clay-Polymer Complex*, Elsevier, Amsterdam (1979).
14. B. Theng, *Chemistry of Clay-Organic Reactions*, Wiley, New York (1974).
15. K. Yasue, T. Tamura, S. Katahira, and M. Watanabe(to Unitika Ltd), "Reinforced Polyamide Resin Composition and Process For Producing the Same", U.S. Patent 5,414,042 (1995).
16. Y. Kojima, A. Usuki, M. Kawasumi, A. Okada, Y. Fukushima, T. Kurauchi, and O. Kamigaito, *J. Mater. Res.*, **8**, 1179 (1993).
17. Y. Kojima, A. Usuki, M. Kawasumi, A. Okada, T. Kurauchi, and O. Kamigaito, *J. Polym. Sci. Part A: Polym. Chem.*, **31**, 983 (1993).
18. R.A. Vaia, "Polymer Intercalation in Mica-Type Layered Silicates," PhD Thesis, Cornell University, Ithaca, NY (1995).
19. L.A. Utracki, M. Sepehr, and J. Li, *Int. Polym. Process.*, **21**, 3 (2006).
20. A.W. Hofmann, *Liebigs Ann. Chem.*, **78**, 253 (1851).
21. W. Lertwimolnun and B. Vergnes, *Polym. Eng. Sci.*, **46**, 314 (2006).
22. H.R. Dennis, D.L. Hunter, D. Chang, S. Kim, J.L. White, J.W. Cho, and D.R. Paul, *Polymer*, **42**, 9513 (2001).
23. A. Ziabicki, *Prog. Colloid Polym. Sci.*, **92**, 1 (1993).
24. L. Zhu and M. Xanthos, *J. Appl. Polym. Sci.*, **93**, 1891 (2004).
25. Y. Wang, F.-B. Chen, and K.-C. Wu, *J. Appl. Polym. Sci.*, **93**, 100 (2004).
26. J. Li, M.-T. Ton-That, and S. Tsai, *Polym. Eng. Sci.*, **46**(8), 1060 (2006).
27. L.A. Utracki and R. Simha, *Macromolecules*, **37**, 10123 (2004).
28. Q. Yuan and R.D.K. Misra, *Polymer*, **47**, 4421 (2006).

 DOI 10.1002/pen